

Article

Damage Detection and Analysis of Urban Bridges Using Terrestrial Laser Scanning (TLS), Ground-Based Microwave Interferometry, and Permanent Scatterer Interferometry Synthetic Aperture Radar (PS-InSAR)

Xianglei Liu ¹, Peipei Wang ¹, Zhao Lu ¹, Kai Gao ¹, Hui Wang ¹, Chiyu Jiao ² and Xuedong Zhang ^{1,*}

¹ Key Laboratory for Urban Geomatics of National Administration of Surveying, Mapping and Geoinformation, Beijing University of Civil Engineering and Architecture, 1 Zhanlanguan Road, Beijing 100048, China; liuxianglei@bucea.edu.cn (X.L.); wangpeipei@stu.bucea.edu.cn (P.W.); luzhao@stu.bucea.edu.cn (Z.L.); gaokai@stu.bucea.edu.cn (K.G.); wanghui@stu.bucea.edu.cn (H.W.)

² School of Civil and Transportation Engineering, Beijing University of Civil Engineering and Architecture, 1 Zhanlanguan Road, Beijing 100048, China; jcy@bucea.edu.cn

* Correspondence: zhangxuedong@bucea.edu.cn; Tel.: +86-10-61209341

Received: 18 January 2019; Accepted: 4 March 2019; Published: 9 March 2019



Abstract: This paper presents a practical framework for urban bridge damage detection and analysis by using three key techniques: terrestrial laser scanning (TLS), ground-based microwave interferometry, and permanent scatterer interferometry synthetic aperture radar (PS-InSAR). The proposed framework was tested on the Beishatan Bridge in Beijing, China. Firstly, a Digital Surface Model (DSM) of the lower surface of the bridge was constructed based on the point cloud generated by using TLS to obtain the potential damage area. Secondly, the dynamic time-series displacement of the potential damage area was acquired by ground-based microwave interferometry, and the Extreme-Point Symmetric Mode Decomposition (ESMD) method was applied to detect damages by the use of signal decomposition and instantaneous frequency calculation. Lastly, the PS-InSAR technique was applied to obtain the surface deformation around Beishatan Bridge by using COSMO-SkyMed images with a ground resolution of 3 m × 3 m, and finally, we analyzed the causes of bridge damage. The experimental results showed that the proposed framework can effectively obtain the potential damage area of the bridge by the DSM from the point cloud by TLS and further judge whether the bridge was damaged by the ESMD method, based on the time-series displacement data. The results also showed that the subway shield construction may be the reason for damage to Beishatan Bridge.

Keywords: terrestrial laser scanning (TLS); ground-based microwave interferometry; permanent scatterer interferometry synthetic aperture radar (PS-InSAR); extreme-point symmetric mode decomposition (ESMD); instantaneous frequency

1. Introduction

As an important component of allowing the movement of vehicles over and around obstructions in cities, urban bridges not only support the dense flow of traffic but also often are a part of a complex surrounding environment, influenced by subway construction crossing. The safe operation of urban bridges is becoming an increasingly important issue [1]. Together, factors such as age, traffic congestion, vehicle overloading, frequent wind loads, environmental degradation, and climatic catastrophes, over an extended period of time, have inevitably increased the deterioration of urban

bridges in recent years, which can ultimately lead to the reduction of their load carrying capacity, or even sudden collapse, whether or not they are properly maintained [2,3]. Safe operation of urban bridges is vital to human activity in terms of the economy, mobility, and community development [4]. Therefore, it is necessary to have ways to detect damage to safeguard the operational safety of urban bridges, especially for those urban bridges that potentially have damage.

At present, for the purpose of damage detection of urban bridges, the main measurement method is to perform dynamic testing under ambient excitation to obtain the dynamic responses of urban bridges in service [5]. Typical experimental tests are usually carried out using piezoelectric accelerometers, fiber optic sensors, and strain and inductive gauges, which are quite accurate and reliable [6,7]. Nevertheless, these gauges need to be fixed in specific positions on the urban bridges on which they are used. This requirement can give rise to accessibility problems, often requiring the use of scaffolds. Furthermore, these gauges also require hardwiring from the transducers to the data acquisition system, which is a time-consuming and expensive task [8]. In this context, non-contact measurement techniques, such as Global Positioning Systems (GPS) and Close-range Photogrammetry (CP), have been very attractive for bridge measurements. However, the accuracy and low sampling frequency of GPS is not good enough to meet the strict measurement requirements [8,9]. The application of CP is restricted due to the requirement of a large number of cameras installation of fixed reflective points, a complicated control network layout, and massive image data processing [2,10]. For these reasons, ground-based microwave interferometry is a good alternative technique, as it uses radar working at the Ku-band (12–18 GHz), which facilitates precise measurements. By regarding the reflected points of an electromagnetic wave as a series of virtual sensors, this technique can strongly reduce or even nullify the use of the traditional point sensors, whose positioning involves the use of cumbersome and costly scaffolding, which is occasionally built under hazardous conditions [11]. Many accuracy comparison experiments, using ground-based microwave interferometry and accelerometers, have been performed on the dynamic monitoring of various large bridges. The results showed that the differences in the displacements of these bridges were in the order of one-tenth of millimeters [11–13]. Therefore, because of the great advantages of non-contact measurements, their wide frequency range of response, their sub-millimetric displacement sensitivity, and their quick set-up, ground-based microwave interferometry has been used for non-contact vibration and displacement monitoring of various bridges [8,14–16]. However, as a linear measurement technique for ground-based microwave interferometry, it is difficult to pinpoint the location of the damage to obtain accurate time-series displacement for urban bridges.

Moreover, besides dynamic testing under ambient excitation to detect damage in urban bridges, traditional point-wise surveying methods are mostly used for periodic deformation monitoring for urban bridges, such as levelling and tacheometry [17]. Although these techniques can provide a high accuracy for deformation measurement, on urban bridges they are limited to measuring a small number of points because it is difficult to reflect the entire deformation and, further, to identify the parts of the bridge that are damaged. Therefore, due to their ability to provide point clouds over the bridge surface with millimeter accuracy, CP and Terrestrial Laser Scanning (TLS) have been widely applied for periodic deformation monitoring of urban bridges in recent years [3]. CP is a remote measuring technique, which uses digital photogrammetry and dense image-matching algorithms, to produce point clouds over the surface of bridges, and analyze bridge deformation by three-dimensional (3D) reconstruction based on the acquired point clouds [10,18,19]. However, CP is a scale-independent measurement technique, of which the resulting raw models need to be post-processed and scaled in order to produce suitable 3D models. This requires a control network of many known targets or natural points on the surface of the monitored bridges to be digitized, which is a time-consuming task, or even too difficult to be implemented [20]. TLS is a ground-based technique that automatically collects the 3D spatial coordinates of a large amount of points of objects in a very short period of time [21]. In this method, a laser beam is emitted from a laser light source and used to scan the surface of surrounding objects in a raster-wise manner. The main advantage of the deformation monitoring by TLS is its full

surface 3D representation; other advantages of TLS include non-contact long-range measurements, a high degree of automation, easy-to-use hardware, and intensive sampling capability [22]. TLS has been introduced for the deformation monitoring of different applications in the fields of architecture, civil engineering, manufactory, and archaeology [22–25].

When it is determined that an urban bridge has damage or potential damage, it is always important to seek the cause or causes of the damage, so that monitoring can be used for future preventative maintenance of the bridge. Relevant studies have shown that the causes of urban bridge damage are often closely related to the surrounding environment [26,27]. Differential Interferometry Synthetic Aperture Radar (D-InSAR) is a technique that obtains large-scale surface micro-deformation information from space [28]. Its main advantage is that it can perform all-day and all-weather observations. The D-InSAR technique is the result of the quantitative development of remote sensing, especially microwave remote sensing, and is a scientific practice of “data to information, information to knowledge”. However, with the continuous deepening of D-InSAR research, some disadvantages of traditional D-InSAR, such as temporal decorrelation, spatial decorrelation, and atmospheric interference, which limit the application of D-InSAR, have gradually been exposed [29,30]. Therefore, to overcome these problems, researchers proposed Permanent Scatterer InSAR (PS-InSAR) [29]. This method overcomes the influence of atmospheric effects and decorrelation of the traditional D-InSAR and ensures that the method can be used even when baselines of several pairs of acquisitions exceed the critical baseline, because there are many pairs that can be formed when dozens of acquisitions are used. Compared to leveling and GPS technology, PS-InSAR can obtain a long-term series of surface deformation values for ten years using only dozens of scenes. The density of PS points is much larger than the density of data points obtained by traditional leveling and GPS measurement methods. This method not only reduces costs, but also guarantees enough precision for ground deformation monitoring, which has been validated by the leveling and GPS technology [30]. Therefore, in the last few decades, PS-InSAR has been widely exploited in many fields, such as surface subsidence, the deformation monitoring of buildings, and the detection of bridges [31–34].

The objective of this paper is to present a framework for damage detection and analysis of urban bridges by using TLS, ground-based microwave interferometry, and PS-InSAR. TLS is applied to obtain the 3D deformation map to find the potential damage area of urban bridges. Ground-based microwave interferometry is used to obtain the dynamic time-series displacement of the potential damage area of urban bridges under the ambient excitation of the passage of vehicles and to further analyze the damaged locations of urban bridges by the extreme-point symmetric mode decomposition (ESMD) method. PS-InSAR is applied to analyze the cause or causes of bridge damage. The rest of this paper is organized as follows. The study site is described in Section 2. Section 3 introduces the measurement methods. Section 4 presents the experimental results and discussion, followed by the conclusions in Section 5.

2. Study Site

Built in 1996, the G6 motorway is one of the most important terrestrial modes of transportation in the northwest region of China. It has approximately 2618 km of transportation infrastructure (including pavements, culverts, and bridges) in use between Beijing and Lhasa. As shown Figure 1, the bridge used as the test subject in this study, Beishatan Bridge, is the way connected to the G6 motorway, which is located between the North Fourth Ring and the North Fifth Ring in Beijing. As shown in Figure 2, the Beishatan Bridge is composed of two sub-bridges, the right sub-bridge (direction to Beijing) and the left sub-bridge (direction from Beijing), which have the same length and width. As shown in Figure 3, a sub-bridge is an 86.58 m continuous girder bridge, which is divided into three spans, including a main span of 40 m and two side spans of 19.6 m and 26.98 m (Figure 3a). The width of the girder is 12.93 m, with three web center lines (Figure 3b). Aiming to safeguard the operational safety of this bridge, periodic monitoring was performed by a total station. As shown in Figure 3a, the nine monitoring points, 1 to 9, were designated on the lower surface of Beishatan Bridge

along the vertical section. As shown in Figure 3b, three monitoring points were designated on the lower surface of the bridge along the cross section. However, in October 2016, the monitored results showed that a maximum deflection of approximately 8 cm occurred at the location of point 5 along direction of the web center line containing point 11 for the right sub-bridge, which was approximately 3 cm according to the last periodic monitoring. In order to avoid further deterioration of the right sub-bridge of Beishatan Bridge, the right sub-bridge of the Beishatan bridge was supported by jacks, as shown in Figure 2. Therefore, it is urgent to obtain an accurate damage area and the causes of bridge damage and to facilitate for bridge reinforcement and maintenance.

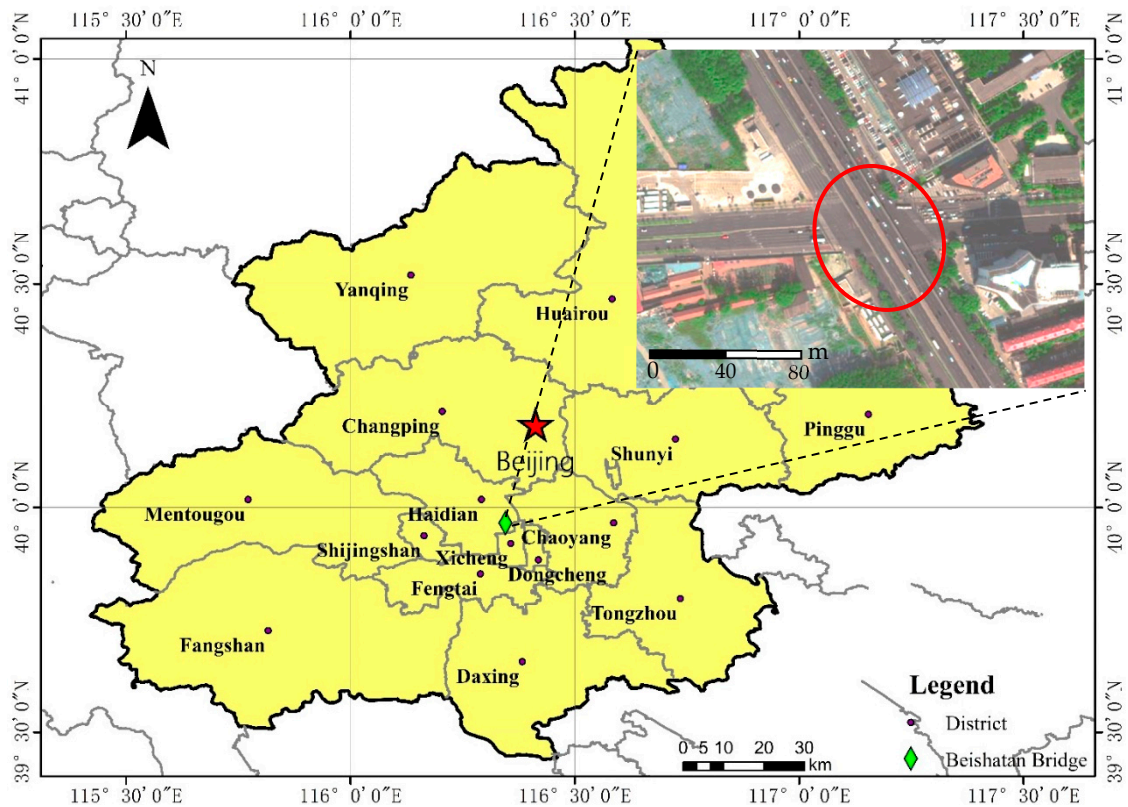


Figure 1. The study area of Beishatan Bridge located in Beijing, China.



Figure 2. Statue of Beishatan Bridge.

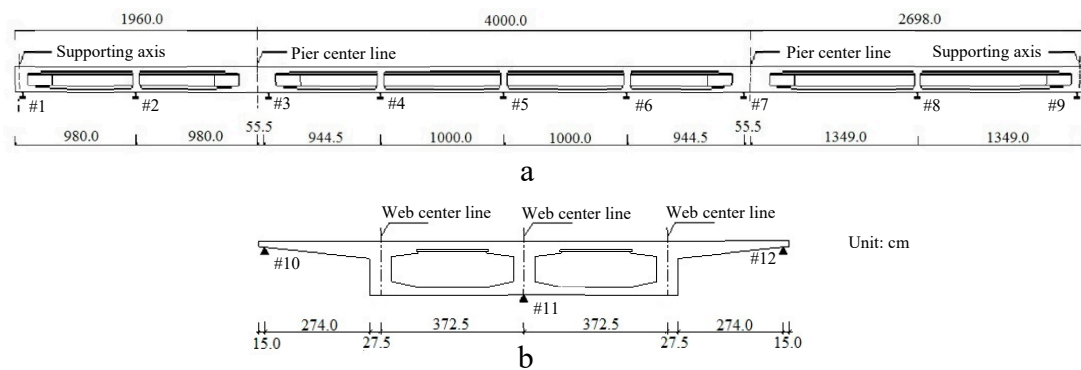


Figure 3. Sketch of Beishatan Bridge. (a) vertical section and (b) cross section.

3. Methods

Figure 4 shows the entire technical framework of damage detection and analysis of urban bridges via TLS, ground-based microwave interferometry, and PS-InSAR; this framework consists of the following three steps. The first step is to find the potential damage area of urban bridges by the use of TLS technique. The second step is to perform damage detection from the potential damage area of the urban bridge by using the ESMD method, which is based on the time-series displacement under ambient excitation of the passage of vehicles through the use of ground-based microwave interferometry. The last step is to analyze the cause of the bridge damage by using the PS-InSAR technique.

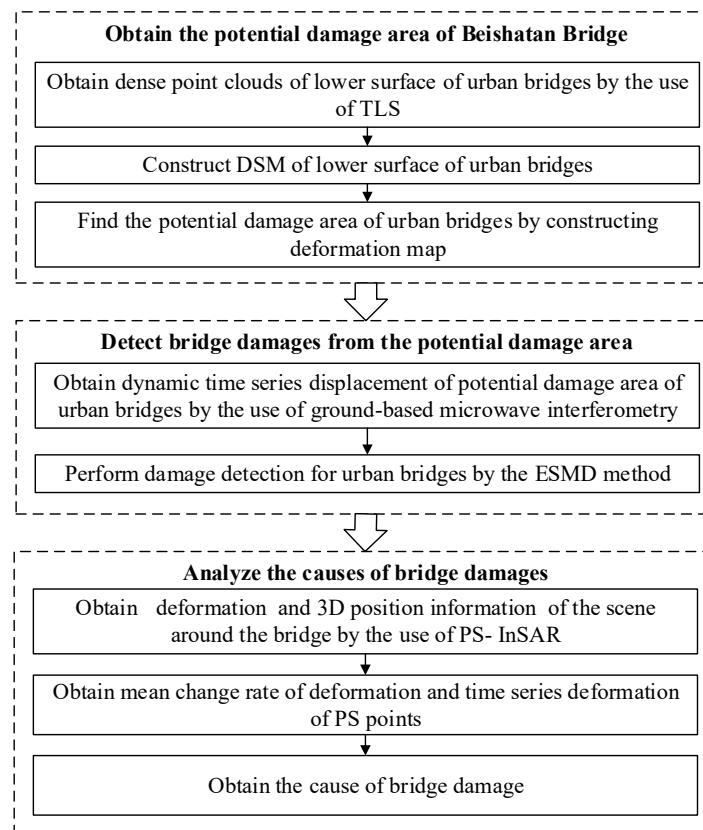


Figure 4. The technological framework of detecting bridge damage areas and damage causes. TLS, terrestrial laser scanning; DSM, digital surface model; ESMD, extreme-point symmetric mode decomposition; PS-InSAR, permanent scatterer interferometry synthetic aperture radar.

3.1. Potential Damage Area Acquired by Using TLS

In this study, according to the previously monitored results by a total station, there was a maximum deflection of approximately 8 cm that occurred at the location of point 5 on the right sub-bridge. However, as shown in Figure 3, only nine monitoring points were designated on the lower surface of the Beishatan Bridge along the vertical section. It is difficult to fully reflect the deformation of Beishatan Bridge, and any monitoring technique needs to acquire accurate damaged location and deformation information with a millimeter scale accuracy. Therefore, with the advantages of a scanning speed of up to 300,000 points per second, a wide field-of-view of $60^\circ \times 360^\circ$, an angle resolution of up to 0.0005° , and a scanning accuracy of 5 mm within a range of 100 m, a TLS Riegl VZ-1000 (RIEGL Laser Measurement Systems GmbH, Horn, Austria) was used to perform deformation measurements to obtain the potential damage area for the main span of the Beishatan Bridge [35]. As shown in Figure 5a, 12 scanning stations were evenly designated around or under the bridge. Four of 12 points, namely points 1, 4, 5, and 8, were set around the bridge with a horizontal distance of approximately 8.2 m from the measuring center of the Riegl VZ-1000 to the bridge, as shown in Figure 5b, and eight other points were set under Beishatan Bridge, with a vertical distance of approximately 4.1 m from the measuring center of the Riegl VZ-1000 to the bridge and a horizontal distance of about 2 m from the measuring center of Riegl VZ-1000 to the Pillars, as shown in Figure 5c. The obtained point clouds from the 12 scan stations were registered using a Riscan Pro (a companion software for RIEGL Terrestrial 3D Laser Scanner Systems) with two steps. The first step was rough registration based on sampling consistency to provide initial estimation of rigid body transform by selecting at least four corresponding points between two adjacent scan stations; the second step was fine registration by using multi-station adjustment [36]. After that, a digital surface model (DSM) of the lower surface of Beishatan Bridge was constructed by using the registered point cloud, which can be used to acquire the potential damage area of the monitored bridge by using comparative analysis between the two sub-bridges. The area with a severe differential subsidence can be considered as the potential damage area of the monitored bridge.

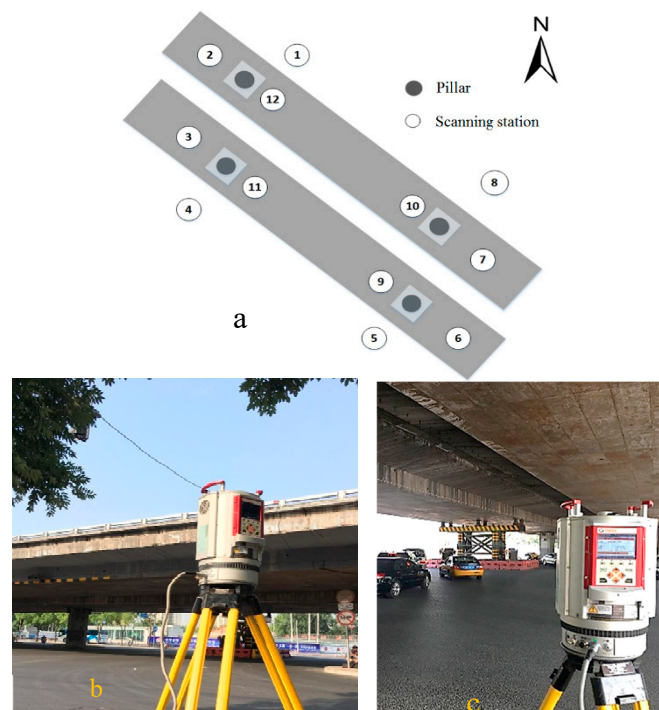


Figure 5. Layout of the Riegl VZ-1000 for the potential damage area acquisition. (a) 12 scanning stations around or under Beishatan Bridge, (b) scanning station 5 around Beishatan Bridge, and (c) scanning station 11 under Beishatan Bridge.

3.2. Damage Detection Based on Time-Series Displacement by Ground-Based Microwave Interferometry

To detect damage from the potential damage area of Beishatan Bridge, the used dynamic time-series displacements need to reach a submillimeter accuracy. Therefore, an Image By Interferometric Survey of Structures (IBIS-S) was applied to acquire an accurate dynamic time-series displacement of the potential damage area. An IBIS-S instrument is a typical sensor that uses ground-based microwave interferometric techniques for the remote dynamic monitoring of urban bridges in any weather conditions, independent of daylight. The IBIS-S consists of a radar unit, a control PC, a power supply unit, and a tripod [37]. The core component of the IBIS-S instrument is a radar unit, which generates, transmits, and receives the electromagnetic signals, and processes the preserved phase information of the received signals to calculate the displacement of the monitored objects [38,39]. Using the Stepped-Frequency Continuous Wave (SF-CW) technique, the IBIS-S has the capability of long-distance transmission and a higher range resolution of up to 0.5 m, without installation of multiple units on the monitored objects [40,41]. Using microwave interferometry technique, the IBIS-S can ensure a higher displacement accuracy of up to 0.01 mm [39]. Moreover, with a sampling rate of up to 200 Hz to sample the scenario, the IBIS-S instrument is suitable for bridge dynamic monitoring, whose significant frequency content of displacement is in the range of approximately 0–10 Hz for bridges [8]. As shown in Figure 6a, for the right sub-bridge of the Beishatan Bridge, the IBIS-S instrument was located on one side of the bridge; the radar unit's angle of altitude was 32° , which was aligned to the suspected damage area. Aiming to evaluate and validate the results of the right sub-bridge, as shown in Figure 6b, the layout of the IBIS-S instrument on the left bridge was similar to that of the right sub-bridge for the time-series displacement measurement. Furthermore, providing a measurement of the line-of-sight displacement using IBIS-S requires prior knowledge of the direction of motion to evaluate the actual dynamic deflection, which can be calculated by making straightforward geometric projections [40].

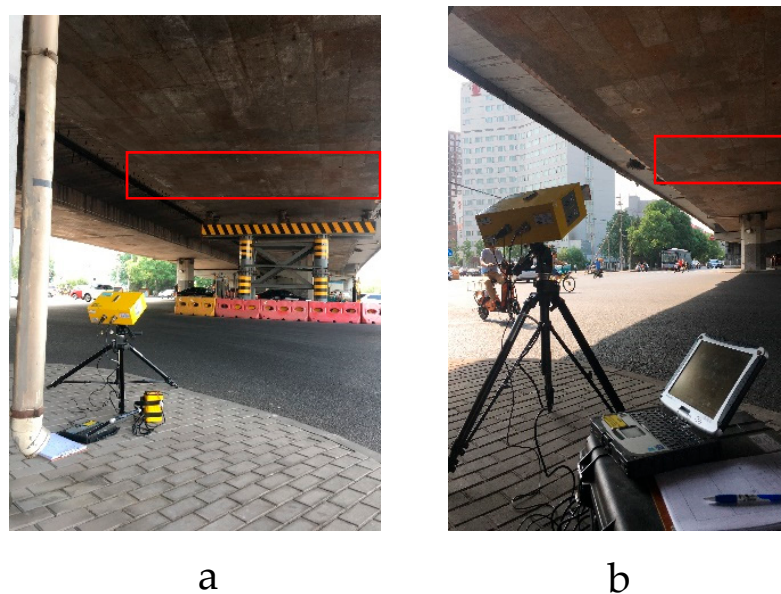


Figure 6. Layout of IBIS-S for time-series displacement acquisition. (a) layout of IBIS-S for time-series displacement acquisition of the right sub-bridge, and (b) layout of IBIS-S for time-series displacement acquisition of the left sub-bridge.

Generally speaking, under the ambient excitation of passing vehicles, there should be non-stationary and non-linear signals for the obtained time-series displacement of damaged bridges [42]. The ESMD method is a new alternative to the Hilbert-Huang Transform (HHT) with the advantage of determining an optimal global mean curve in an adaptive way, to decompose a complicated response signal into a series of finite and small Intrinsic Mode Functions (IMFs) [43].

Compared with HHT, this method not only reduces the difficulty of determining the sifting time, but also determines the instantaneous frequency and amplitude in a direct interpolation algorithm, which can reconcile the conflict between the period and frequency [44]. To date, the ESMD method has been gradually applied in the field of structural damage detection [44,45]. Therefore, this paper uses the ESMD method to detect damage from the potential damage area of Beishatan Bridge, based on the obtained non-stationary and non-linear signals received by ground-based microwave interferometry. The detailed steps are shown as follows: (1) Decompose the time-series displacement of the potential damage area obtained by ground-based microwave interferometry into a series of IMFs by using the ESMD method, (2) obtain the instantaneous frequency of the corresponding each decomposed IMF by the direct interpolation algorithm [45], and (3) detect bridge damage according to the reduction of instantaneous frequency.

3.3. Damage Analysis by PS-InSAR

In order to grasp and analyze the damage to the Beishatan Bridge and its causes from a macroscopic perspective, we need to acquire accurate time-series deformation information with a millimeter scale accuracy. Therefore, this paper used a PS-InSAR technique to monitor the ground surface deformation of the Beishatan Bridge and its surrounding area. Unlike the D-InSAR processing method, which is based on a single interference image pair, PS-InSAR uses multiple SAR images that cover the same region to perform time-series phase differential interference and selects a pixel subset with stable phase quality as the main processing object. According to the space-time characteristics of each phase component, this technique can be used to estimate atmospheric fluctuations, Digital Elevation Model (DEM) errors, and noise, which can be separated from the differential interference phases one-by-one. Then, the linear and nonlinear deformation rates of each PS can be obtained together with Atmosphere Phase Screen (APS) and DEM errors. In this study, 61 SAR images acquired from the Italian COSMO-SkyMed, a constellation composed of four satellites equipped with SAR operating at the X-band, were taken as the source data, which covered the main city in Beijing from 2011 to 2017. Specific parameters of the SAR images are shown in Table 1. The first SAR image was selected as the master image, the other SAR images were registered with it, and an interference image pair was established. All the interference image pairs were subjected to phase difference processing to form an interferogram sequence. Then, more than 12.6 million stable PS points were obtained by computing the phase information of the images with a distribution density of approximately 20,000 PS points per square kilometer. At last, establishing the function of deformation and phase difference based on the PS points can effectively reduce the influences of data errors and atmospheric delay errors for the PS points, and further obtain accurate surface subsidence information, as shown in Figure 7. Then, the causes of bridge damage can be analyzed based on the time-series of ground subsidence and average subsidence rates from the selected PS points around the monitored bridge.

Table 1. Technical specifications of the synthetic aperture radar (SAR) data in the experiment.

Item	Value
Satellite	COSMO-SkyMed
Coverage area	40 × 40 km ²
Imaging mode	Stripmap
Ground resolution	3 m × 3 m
Polarization mode	HH
Incident angle	~20.07 °
View direction/orbit	Right view/descending orbit
Amount of data	61
Time span	January 2011–February 2017

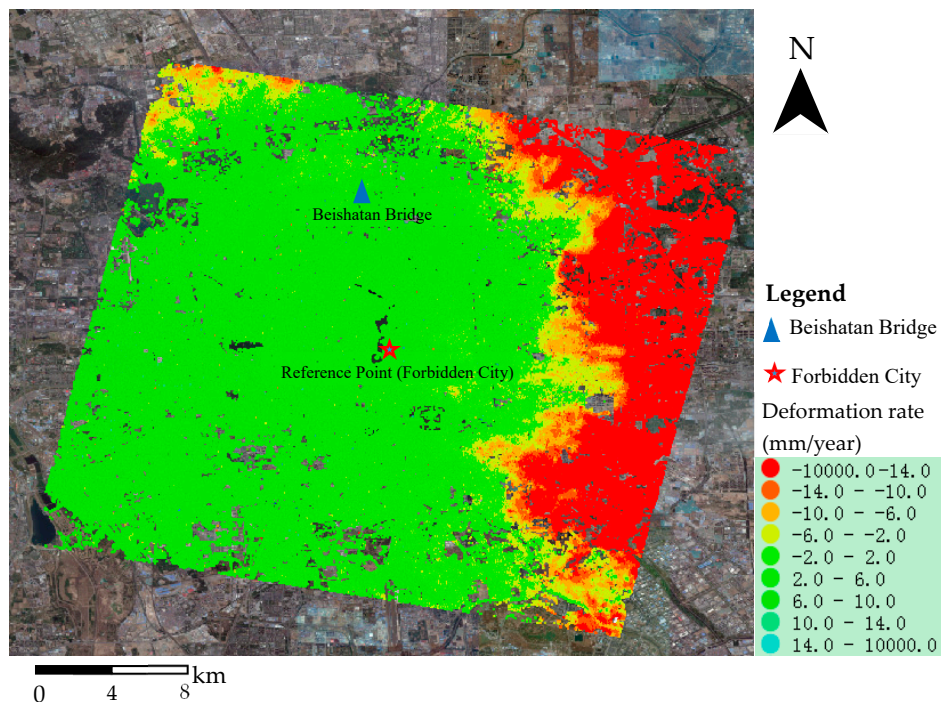


Figure 7. Permanent scatterer (PS) deformation rate map of the whole image in the test area.

4. Experimental Results and Discussions

4.1. Results and Analysis of Bridge Deformation

As shown in Figure 8, the DSM of the lower surface of the Beishatan Bridge was constructed from the point clouds obtained by TLS. The inspection of elevation of the lower surface of the Beishatan Bridge from this figure clearly highlights the following: (1) For the side-spans L1 and R1 of the left and right sub-bridges shown in Figure 8a, the average elevation values were 3.243 m and 3.242 m, respectively, and the trend of elevation of DSMs was basically consistent. Therefore, a conclusion can be made that damage did not occur in these two side-spans. (2) For the side-spans L3 and R3 of the left and right sub-bridges shown in Figure 8a, the trend of elevation of DSMs was basically consistent, but the average elevation value was 3.226 m for the right sub-bridge, which was less than the 3.241 m of the left sub-bridge. These results showed that the overall subsidence may have occurred in the right sub-bridge. (3) For the mid-spans L2 and R2 of the left and right sub-bridges, as shown in Figure 8a, the average elevation values were 3.281 m and 3.234 m, respectively. There was an average elevation difference of approximately 5 cm. Furthermore, the trend of elevation of DSMs was inconsistent for the left and right sub-bridges. As the trend of the designed elevations is a gradual process like the left sub-bridge shown in Figure 8 and is basically the same for the left and right sub-bridges, there was a differential subsidence in the mid-spans of the right sub-bridge. Generally, differential subsidence may cause cracks in the surface of the monitored bridge [26]. However, as shown in Figure 9, there are no cracks in the lower surface of the right sub-bridge; therefore, some damage may have occurred inside the mid-span of the right sub-bridge, which is in the initial stage of bridge damage. The results demonstrate that the TLS technique is an effective technique to find out the potential damage area of the monitored bridge caused by differential subsidence, whether there are cracks in the bridge surface or not, which is a great advantage compared with the traditional point-wise surveying methods. However, it is difficult to acquire the potential damage area caused by the abnormal stress of the foundation structure and the tilting and sliding of the bridge foundation.

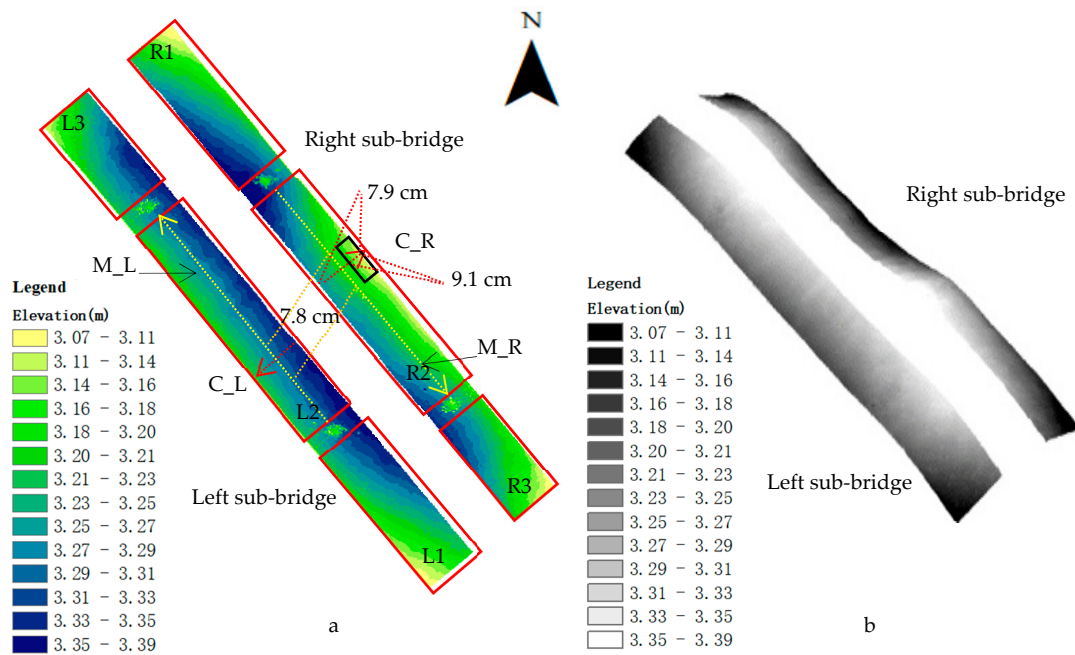


Figure 8. DSM of the lower surface of the Beishatan Bridge. (a) 2D DSM of the lower surface of the Beishatan Bridge, and (b) 3D DSM of the lower surface of the Beishatan Bridge.



Figure 9. Statue of the lower surface of the right sub-bridge of Beishatan Bridge. (a) the southern half of the right sub-bridge of Beishatan Bridge, and (b) the north half of the right sub-bridge of the Beishatan Bridge.

In order to obtain the maximum deformation region of the mid-span of the right sub-bridge, and further determine the potential damage area for dynamic time-series displacement acquisition by ground-based microwave interferometry, a longitudinal section line (LSL) and a cross section line (CSL) were extracted from the DSM of the lower surface of the Beishatan Bridge, as shown in Figure 10. The elevation changes from this figure clearly highlight the following: (1) As shown in Figure 10a, an LSL along the midline of each bridge (yellow dotted line in Figure 8a) was extracted from the DSM of the left and right sub-bridges. Compared with the left bridge, there is an obvious deformation that occurred in the right sub-bridge, with an average difference of approximately 5.4 cm. Especially, in the range of approximately 10–18 m along the midline of the bridges, shown as the black box in Figure 10a,

the average elevation difference is as high as approximately 7.8 cm, which can be regarded as a potential damage area. (2) As shown in Figure 10b, aiming to determine the accurate damage area, a CSL (red dotted line in Figure 8a), located at 14 m along the direction of the LSL of each bridge, was extracted from the DSM of the left and right sub-bridges. Obviously, there was a greater elevation difference between the CSLs of C_L and C_R of the two bridges, with an average elevation difference of approximately 7.9 cm, especially for the outer side of the bridges shown in Figure 10b as the black box; the elevation difference was gradually increased up to 9.1 cm. Therefore, the outer side of the right sub-bridge in the range of approximately 10–18 m along the midline of bridges is the most likely damage area, as shown as the black box in Figure 8a.

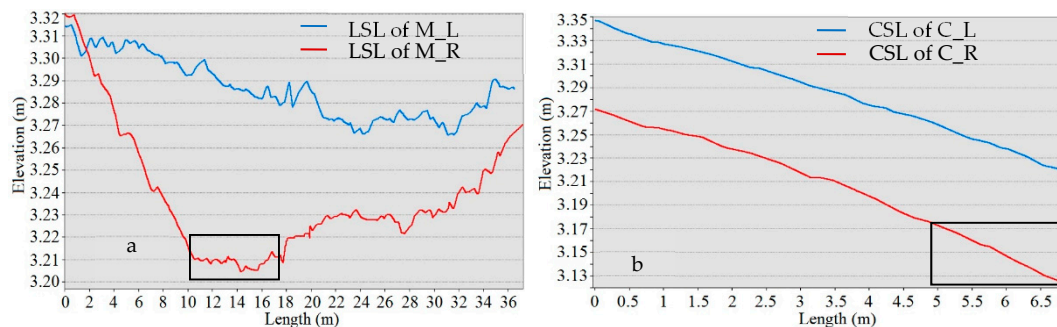


Figure 10. Curves of a longitudinal section line (LSL) and a cross section line (CSL) extracted from the DSM of bridges. (a) the LSL curves of M_L and M_R extracted from the DSM of the left and right sub-bridges along the midline, and (b) the CSL curves of C_L and C_R extracted from the DSM of the left and right sub-bridges at the location of 14 m along the direction of LSLs.

4.2. Damage Detection Analysis and Discussion

For the purpose of detecting damage from the above potential damage area for the right sub-bridge, a dynamic time-series displacement with a duration of about 37 s, named “Data”, shown in Figure 11a, was obtained by ground-based microwave interferometry in this area; this analysis was undertaken with the transient load of vehicles. Moreover, aiming to make a comparison analysis between the right and the left sub-bridges, a dynamic time-series displacement with a duration of about 29 s, named “Data” shown in Figure 11b, was also obtained by ground-based microwave interferometry for the left bridge in a similar area, as shown in Figure 6. Furthermore, as shown in Figure 11, each set of dynamic time-series displacements was decomposed into seven IMF components (IMF1–IMF7) by use of the ESMD method. The inspection of the IMFs in this figure clearly highlights the following: (1) For the right sub-bridge, there were two obvious variations that appear on the curve of the dynamic time-series displacement, as shown in Figure 11a; the maximum displacements were approximately 0.78 mm and 1.26 mm, which may be caused by the different speeds and weights of the vehicles passing through the bridge. For the left bridge, there were also two displacement variations appearing on the curve of the dynamic time-series displacement, as shown in Figure 11b. However, the maximum displacements were approximately 0.62 mm and 0.41 mm, which were smaller than those of the right sub-bridge. Although different speeds and weights of the vehicles passing through the bridge lead to different maximum displacements, these results also indicate that the right sub-bridge may be more damaged than the left bridge. (2) For the decomposed IMF1 to IMF3 of the right sub-bridge, the displacement variation was in the interval of -0.5 mm to 0.5 mm, which was larger than that of the other four decomposed IMFs. Moreover, there were some obvious sudden variations appearing on the displacement curves of IMF1 to IMF3. These results showed that the decomposed IMF1 to IMF3 are the main components of the original dynamic time-series displacement of the right sub-bridge. Similarly, the decomposed IMF1 to IMF3 of the left bridge are also the main components of the original dynamic time-series displacement.

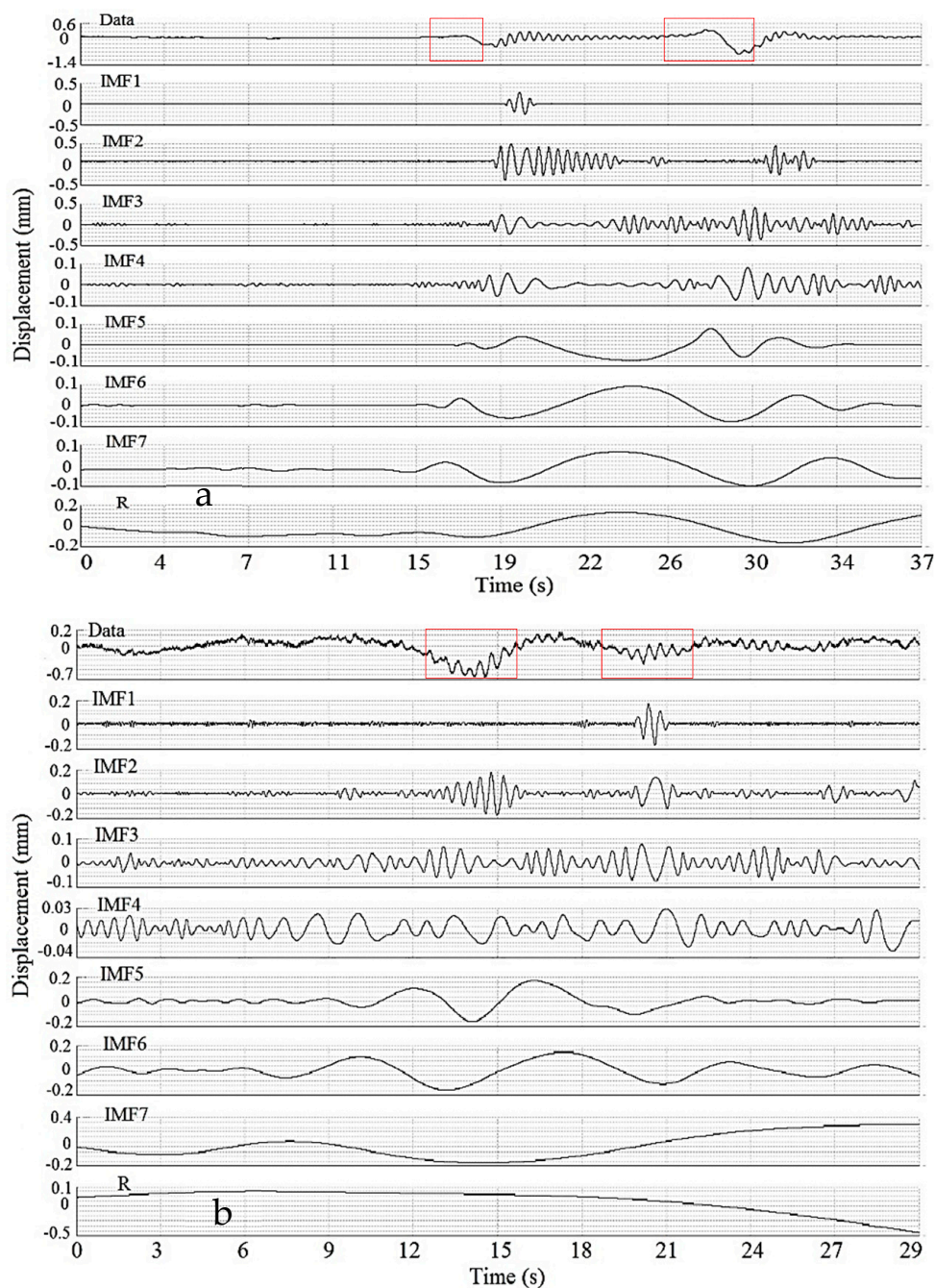


Figure 11. Original dynamic time-series displacement and the corresponding decomposed Intrinsic Mode Functions (IMFs) of the right and left sub-bridges. (a) Original dynamic time-series displacement and the corresponding decomposed IMFs of the right sub-bridge, and (b) original dynamic time-series displacement and the corresponding decomposed IMFs of the left sub-bridge.

Generally, instantaneous frequency is a transient structural vibration response that depends on the structural natural frequency, damping, stiffness, and exciting conditions [46]. Therefore, if there were some existing damage in a certain part of a bridge, the instantaneous frequency, obtained from the dynamic time-series displacement, should be reduced. As shown in Figure 12, the instantaneous frequency and amplitude of each IMF for each set of dynamic time-series displacements was calculated by using the direct interpolation algorithm [45]. The inspection of the instantaneous frequency and amplitude of each IMF in this figure clearly highlights this observation for IF1 to IF3 of the right sub-bridge, as shown in Figure 12a; when the corresponding amplitudes A1 to A3 are larger, there are

obviously reductions of instantaneous frequency in the curves of IF1 to IF3. However, for the IF1 to IF3 of the left sub-bridge, as shown in Figure 12b, there are some obviously larger amplitudes in the curves of A1 to A3, but the distribution is approximately uniform for the obtained instantaneous frequencies of IF1 to IF3. There are no instantaneous frequency reductions in the curves of IF1 to IF3. These results indicate that there is some damage to the right sub-bridge. Moreover, although the contact transducers, including accelerometers, and strain and inductive gauges, can also be used to obtain the accurate and reliable time-series displacement, this process has been proven to be a time-consuming and expensive task [8]. Therefore, the results demonstrate that the ground-based microwave interferometry is a good alternative technique to acquire accurate time-series displacement for damage detection of the monitored bridge, together with the potential damage area obtained by using a TLS technique, although it has a higher price.

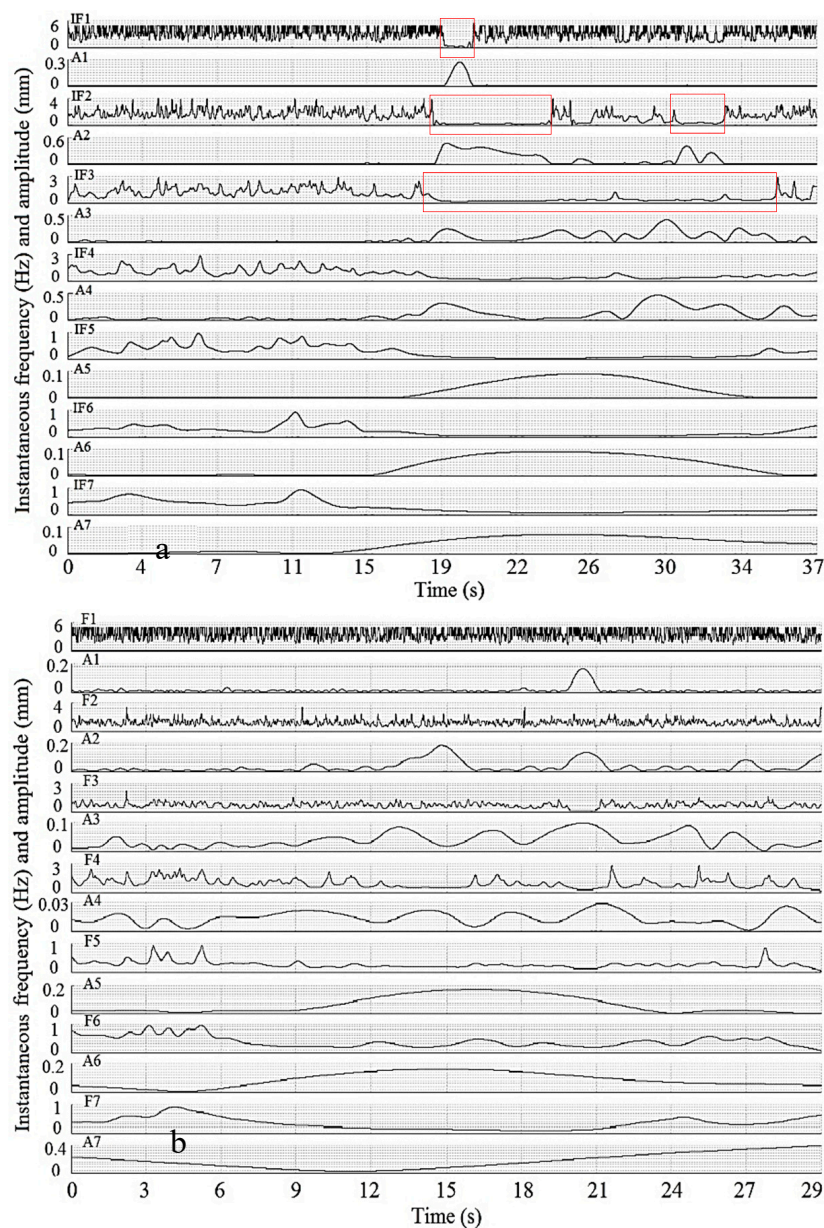


Figure 12. Instantaneous frequency and amplitude of each IMF of the right and left sub-bridges. (a) instantaneous frequency and amplitude of each IMF of the right sub-bridge, and (b) instantaneous frequency and amplitude of each IMF of the left sub-bridge.

4.3. Subsidence Analysis and Discussion

In order to analyze the reasons for damage of the right sub-bridge of the Beishatan Bridge, the ground surface subsidence of key locations around the Beishatan Bridge were obtained by using the PS-InSAR technique, based on 61 SAR images from 2011 to 2017. As shown in Figure 13, eight key locations were selected around the Beishatan Bridge to perform the analysis. Three of them, locations A1 to A3, are in the front, middle, and rear positions on the east side of the right sub-bridge. Locations B1 to B3 are in the left, middle, and right positions on the north side of the Beishatan Bridge, and locations C1 and C2 are in the left, middle, and right positions on the south side of the Beishatan Bridge. The corresponding subsidence curves of the eight locations are shown in Figure 14, and the average subsidence rate of each location is also calculated according to the time interval and subsidence difference between the first and last images [29]. The inspection of the subsidence curves and average subsidence rates of the eight locations in these figures clearly highlights the following: (1) The average subsidence rates at locations A1 and A2 are -3.50 mm/year and -3.09 mm/year, which are greater than the values of location A3, which has a subsidence rate of -1.53 mm/year. Moreover, as described in Sections 4.1 and 4.2, the damaged location of the right sub-bridge of the Beishatan Bridge is between locations A1 and A2. This indicates that ground subsidence may be one of the main reasons for the cause of damages to the right sub-bridge of the Beishatan Bridge. (2) The average subsidence rates at locations B1, B2, and B3 are -7.36 mm/year, -5.14 mm/year, and -8.06 mm/year, respectively. Meanwhile, the average subsidence rates at locations C1 and C2 are -2.47 mm/year and -3.29 mm/year, respectively. Therefore, compared with the south side of the bridge, there is a significant subsidence on the north side of the bridge, which is close to the damaged location of the right sub-bridge of the Beishatan Bridge. These results further indicate that ground subsidence is one of the main causes of damages to the right sub-bridge of the Beishatan Bridge. (3) Moreover, although the subsidence rate of each location is different for each of the eight locations, the variation trend of the eight subsidence curves is basically the same. Especially from the end of 2012 to early 2015, there has been an obvious sharp decrease in all the eight subsidence curves. Therefore, the larger ground subsidence during this period may be the main factor for the damage to the Beishatan Bridge.

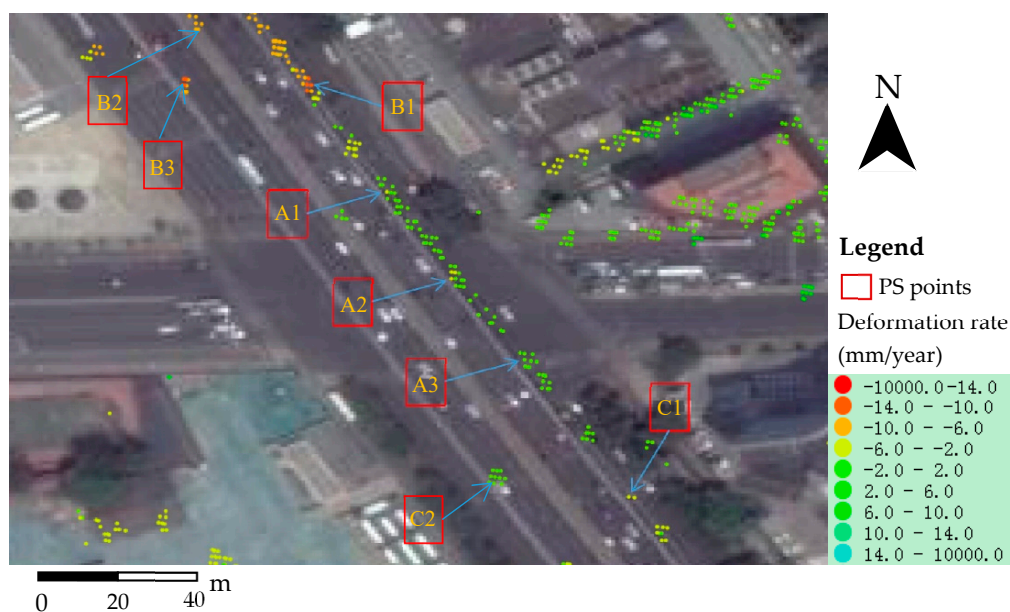


Figure 13. Eight key locations used for subsidence analysis around the Beishatan Bridge.

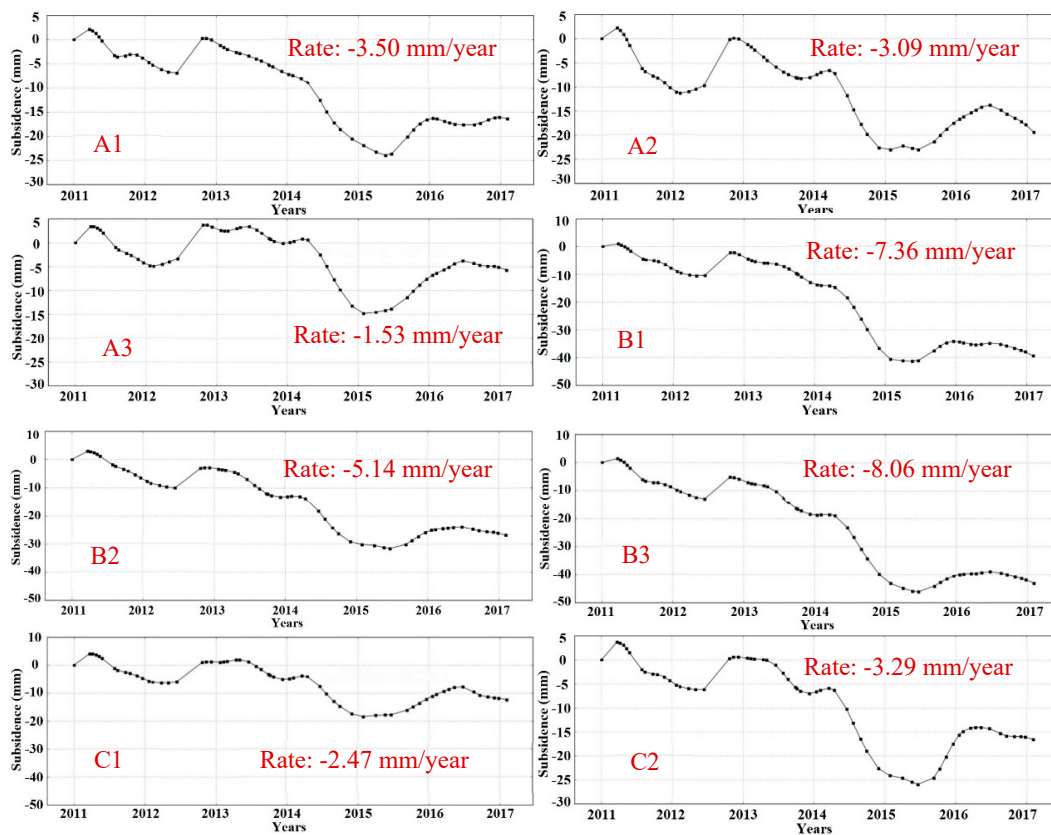


Figure 14. The subsidence curves of eight locations around the Beishatan Bridge.

As shown in Figure 15, there is a subway station on the west side of the Beishatan Bridge. Therefore, four key locations, named S1 to S4, were selected for use in a subsidence analysis related to bridge damage. As shown in Figure 16, the average subsidence rates are -6.06 mm/year, -5.76 mm/year, -4.56 mm/year, and -5.76 mm/year for locations S1 to S4, respectively. They all have a greater subsidence rate, which is close to the value of locations B1 to B3. Moreover, the variation trends of the subsidence curves of locations S1 to S4 are also basically the same as those of the other eight locations around the Beishatan Bridge, which also have an obviously sharp decrease from the end of 2012 to early 2015. Furthermore, aiming to find the main factor causing ground subsidence from the end of 2012 to early 2015, and according to the collected nine images of the Beishatan Bridge at different times from the end of 2012 to early 2015, shown in Figure 17, the subway shield construction period was from September 2012 to December 2015. Obviously, the subway shield construction period is consistent with the timespan of sharp decrease of the subsidence curves for all the above locations. Moreover, as shown in Figure 14, the subway station included four subway exits, S-A, S-B1, S-B2, and S-C. Two of them, S-B1 and S-B2, are at the north side of the Beishatan Bridge. Therefore, the subway shield construction period may be one of the main factors causing the larger ground subsidence for the north side of the Beishatan Bridge, which can cause bridge damages. Moreover, as shown in Figures 14 and 16, there is an obvious uplift in all of the subsidence curves between 2012 and 2013, which was caused by the support structure construction at the beginning of the subway shield construction. The results showed that PS-InSAR, because it has advantages in long time-series, a large scope, and dense 3D measurement, is an effective and reliable technique to analyze the cause of bridge damage caused by differential ground subsidence. However, if the bridge damage is not caused by the differential ground subsidence around the monitored bridge, it is difficult to analyze the causes of bridge damage using the PS-InSAR technique. Moreover, if the terrain around the bridge changes dramatically, it is also difficult to acquire enough PS points to analyze the causes of the bridge damage [47].



Figure 15. Four locations around the subway station at the west side of the Beishatan Bridge.

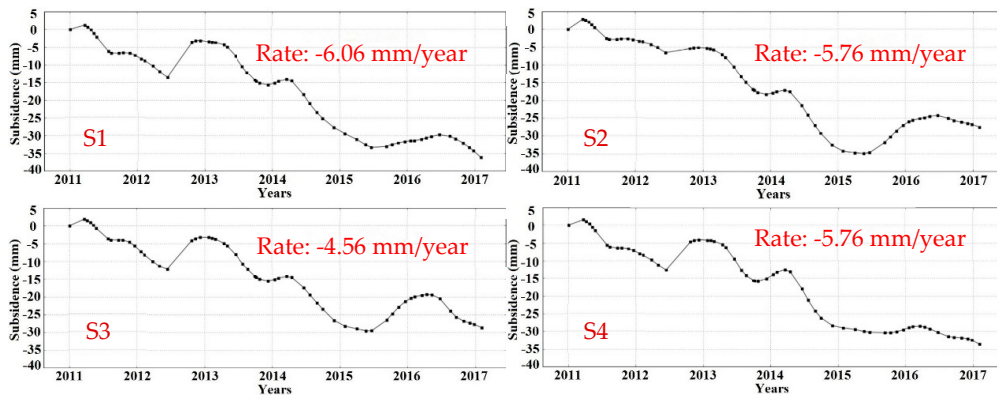


Figure 16. The subsidence curves of four locations around the subway station at the west side of the Beishatan Bridge.

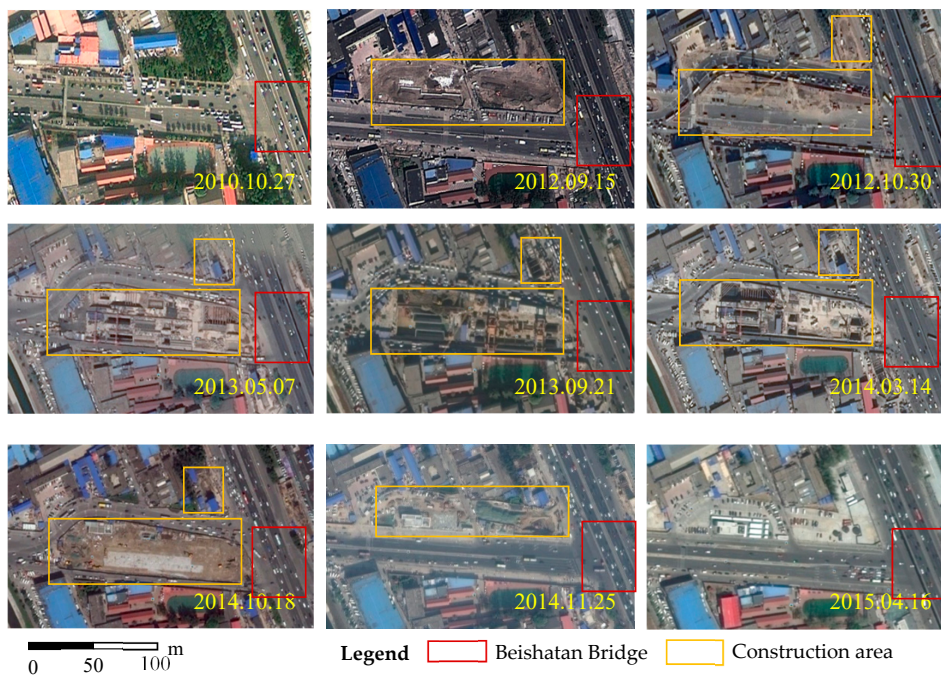


Figure 17. Nine images of the Beishatan Bridge at different times from the end of 2010 to early 2015.

5. Conclusions

To determine the safety status of urban bridges, this study proposed a practical framework to detect and analyze the damage of urban bridges by using TLS, ground-based microwave interferometry, and PS-InSAR. The TLS was applied to obtain the potential damage area. Ground-based microwave interferometry was applied to accurately determine whether the bridge is damaged, and PS-InSAR was applied to analyze the causes of bridge damage. More specifically, the results presented in the paper clearly highlight the following:

(1) Aiming to obtain the potential damage area of urban bridges for further accurate damage detection, with the advantages of non-contact 3D measurement and massive sampling capability, this study used TLS to acquire point clouds of the lower surface of bridges, which was used to construct the DSM of the lower surface of the Beishatan Bridge. Using 2D and 3D deformation maps of the lower surface of the Beishatan Bridge, the potential damage area can be easily obtained according to the differential deformation of the lower surface of the bridge. Moreover, by using the curves of an LSL and a CSL extracted from the DSM of bridges, the most likely damage areas can be obtained. These results show that TLS is an effectively technique to obtain the potential damage areas of bridges.

(2) Aiming to further confirm whether the bridge was damaged in the potential damage areas, an IBIS-S was located on one side of the bridges to acquire an accurate dynamic time-series displacement of the potential damage area for both the right and left sub-bridges of the Beishatan Bridge. The ESMD method was adopted to decompose time dynamic time-series displacement into IMFs for the right and left sub-bridges. By analyzing the relationship between the original dynamic time-series displacement, the main IMF components of the original dynamic time-series displacement were obtained. Furthermore, the instantaneous frequency and amplitude of each IMF for each set of dynamic time-series displacement was calculated by using a direct interpolation algorithm. By analyzing the changes of the instantaneous frequency for the main IMF components, it can be judged whether the monitored bridge was damaged.

(3) Aiming to find the causes of bridge damage for the Beishatan Bridge, the PS-InSAR technique was used to obtain the surface subsidence around the Beishatan Bridge by using 61 SAR images from 2011 to 2017. The results show that the differential settlement caused by the subway shield construction may be the main factors that caused damage to the Beishatan Bridge.

Author Contributions: X.L., C.J. and X.Z. conducted the algorithm design, X.L. and P.W. wrote the paper, and X.L. revised the paper. Z.L., K.G., and H.W. performed the experiment and analyze the results, P.W. and Z.L. contributed to study the proposed algorithm. All authors have contributed significantly and have participated sufficiently to take the responsibility for this research.

Funding: This research was funded by the National Natural Science Foundation of China (grant no. 41871367), the Importation and Development of High-Caliber Talents Project of Beijing Municipal Institutions (grant no. CIT&TCD201704053), the Science and Technology Project of Ministry of Housing and Urban-Rural Development of the People's Republic of China (grant no. 2017-K4-002), the Scientific Research Project of Beijing Educational Committee (grant no. KM201910016005), the Major Projects of Beijing Advanced innovation center for future urban design (grant no. UDC2018031321), the Talent Program of Beijing University of Civil Engineering and Architecture, the Fundamental Research Funds for Central and Beijing Universities (X18051), and the BUCEA Post Graduate Innovation Project.

Conflicts of Interest: The authors declare no conflict of interest.

References

1. Kavvadas, M.J. Monitoring ground deformation in tunnelling: Current practice in transportation tunnels. *Eng. Geol.* **2005**, *79*, 93–113. [[CrossRef](#)]
2. Park, H.S.; Lee, H.M.; Adeli, H.; Lee, I. A new approach for health monitoring of structures: Terrestrial laser scanning. *Comput.-Aided Civ. Inf. C* **2007**, *22*, 19–30. [[CrossRef](#)]
3. Riveiro, B.; González-Jorge, H.; Varela, M.; Jáuregui, D.V. Validation of terrestrial laser scanning and photogrammetry techniques for the measurement of vertical underclearance and beam geometry in structural inspection of bridges. *Measurement* **2013**, *46*, 784–794. [[CrossRef](#)]

4. Alani, A.M.; Aboutaleb, M.; Kilic, G. Applications of ground penetrating radar (GPR) in bridge deck monitoring and assessment. *J. Appl. Geophys.* **2013**, *97*, 45–54. [[CrossRef](#)]
5. Roveri, N.; Carcaterra, A. Damage detection in structures under traveling loads by Hilbert–Huang transform. *Mech. Syst. Signal Process.* **2012**, *28*, 128–144. [[CrossRef](#)]
6. Kai, H.H.; Halling, M.W.; Barr, P.J. Overview of vibrational structural health monitoring with representative case studies. *J. Bridge Eng.* **2006**, *11*, 707–715.
7. Gentile, C.; Bernardini, G. An interferometric radar for non-contact measurement of deflections on civil engineering structures: Laboratory and full-scale tests. *Struct. Infrastruct. E* **2010**, *6*, 521–534. [[CrossRef](#)]
8. Pieraccini, M.; Fratini, M.; Parrini, F.; Atzeni, C. Dynamic monitoring of bridges using a high-speed coherent radar. *IEEE Trans. Geosci. Remote Sens.* **2006**, *44*, 3284–3288. [[CrossRef](#)]
9. Moschas, F.; Psimoulis, P.A.; Stiros, S.C. GPS/RTS data fusion to overcome signal deficiencies in certain bridge dynamic monitoring projects. *Smart Struct. Syst.* **2013**, *12*, 251–269. [[CrossRef](#)]
10. Jiang, R.; Jauregui, D.V. Development of a digital close-range photogrammetric bridge deflection measurement system. *Measurement* **2010**, *43*, 1431–1438. [[CrossRef](#)]
11. Pieraccini, M.; Fratini, M.; Parrini, F.; Atzeni, C.; Partoli, G. Interferometric radar vs. accelerometer for dynamic monitoring of large structures: An experimental comparison. *NDT E Int.* **2008**, *41*, 258–264. [[CrossRef](#)]
12. Gentile, C.; Bernardini, G. Output-only model identification of a reinforced concrete bridge from radar-based measurements. *NDT E Int.* **2008**, *41*, 544–553. [[CrossRef](#)]
13. Gökdağ, H.; Kopmaz, O. A new damage detection approach for beam-type structures based on the combination of continuous and discrete wavelet transforms. *J. Sound. Vib.* **2009**, *324*, 1158–1180. [[CrossRef](#)]
14. Gentile, C. Application of microwave remote sensing to dynamic testing of stay-cables. *Remote Sens.* **2010**, *2*, 36–51. [[CrossRef](#)]
15. Stabile, T.A.; Perrone, A.; Gallipoli, M.R.; Ditommaso, R.; Ponzio, F.C. Dynamic survey of the Musmeci bridge by joint application of ground-based microwave radar interferometry and ambient noise standard spectral ratio techniques. *IEEE Geosci. Remote Sens. Lett.* **2013**, *10*, 870–874. [[CrossRef](#)]
16. Liu, X.; Tong, X.; Ding, K.; Zhao, X.; Zhu, L.; Zhang, X.D. Measurement of Long-Term Periodic and Dynamic Deflection of the Long-Span Railway Bridge Using Microwave Interferometry. *IEEE J. Sel. Top. Appl. Earth Observ. Remote Sens.* **2015**, *8*, 4531–4538. [[CrossRef](#)]
17. Lovas, T.; Barsi, A.; Detrekoi, A.; Dunai, L.; Csak, Z.; Polgar, A.; Berenyi, A.; Kibedy, Z.; Szocs, K. Terrestrial laser scanning in deformation measurements of structures. *ISPRS J. Photogramm.* **2008**, *37*, 527–532.
18. Luhmann, T. Close range photogrammetry for industrial applications. *ISPRS J. Photogramm.* **2010**, *65*, 558–569. [[CrossRef](#)]
19. Ahmadabadian, A.H.; Robson, S.; Boehm, J.; Shortis, M.; Wenzel, K.; Fritsch, D. A comparison of dense matching algorithms for scaled surface reconstruction using stereo camera rigs. *ISPRS J. Photogramm.* **2013**, *78*, 157–167. [[CrossRef](#)]
20. Jiang, R.; Jáuregui, D.V.; White, K.R. Close-range photogrammetry applications in bridge measurement: Literature review. *Measurement* **2008**, *41*, 823–834. [[CrossRef](#)]
21. González-Jorge, H.; González-Aguilera, D.; Rodríguez-Gonzálvez, P.; Arias, P. Monitoring biological crusts in civil engineering structures using intensity data from terrestrial laser scanners. *Constr. Build. Mater.* **2012**, *31*, 119–128. [[CrossRef](#)]
22. Monserrat, O.; Crosetto, M. Deformation measurement using terrestrial laser scanning data and least squares 3D surface matching. *ISPRS J. Photogramm.* **2008**, *63*, 142–154. [[CrossRef](#)]
23. Teza, G.; Galgaro, A.; Moro, F. Contactless recognition of concrete surface damage from laser scanning and curvature computation. *NDT E Int.* **2009**, *42*, 240–249. [[CrossRef](#)]
24. Abellán, A.; Oppikofer, T.; Jaboyedoff, M.; Rosser, N.J.; Lim, M.; Lato, M.J. Terrestrial laser scanning of rock slope instabilities. *Earth Surf. Proc. Land.* **2014**, *39*, 80–97. [[CrossRef](#)]
25. Yang, H.; Omidalizarandi, M.; Xu, X.; Neumann, I. Terrestrial laser scanning technology for deformation monitoring and surface modeling of arch structures. *Compos. Struct.* **2016**, *169*, 173–179. [[CrossRef](#)]
26. Huang, Y.; Jiang, X. Field-observed phenomena of seismic liquefaction and subsidence during the 2008 Wenchuan earthquake in China. *Nat. Hazard.* **2010**, *54*, 839–850. [[CrossRef](#)]
27. Milillo, P.; Giardina, G.; DeJong, M.J.; Perissin, D.; Milillo, G. Multi-Temporal InSAR Structural Damage Assessment: The London Crossrail Case Study. *Remote Sens.* **2018**, *10*, 287. [[CrossRef](#)]

28. Hamling, I.J.; Hreinsdóttir, S.; Clark, K. Complex multifault rupture during the 2016 Mw 7.8 Kaikōura earthquake, New Zealand. *Science* **2017**, *356*, 7194. [[CrossRef](#)]
29. Ferretti, A.; Prati, C.; Rocca, F. Permanent scatterers in SAR interferometry. *IEEE Trans. Geosci. Remote* **2001**, *39*, 8–20. [[CrossRef](#)]
30. Liu, G.; Jia, H.; Zhang, R. Exploration of Subsidence Estimation by Persistent Scatterer InSAR on Time Series of High Resolution TerraSAR-X Images. *IEEE J. Sel. Top. Appl. Earth Observ. Remote Sens.* **2011**, *4*, 159–170. [[CrossRef](#)]
31. Gernhardt, S.; Bamler, R. Deformation monitoring of single buildings using meter-resolution SAR data in PSI. *ISPRS J. Photogramm.* **2012**, *73*, 68–79. [[CrossRef](#)]
32. Fornaro, G.; Reale, D.; Verde, S. Bridge Thermal Dilation Monitoring with Millimeter Sensitivity via Multidimensional SAR Imaging. *IEEE Geosci. Remote Sci.* **2012**, *10*, 677–681. [[CrossRef](#)]
33. Sousa, J.J.; Bastos, L. Multi-temporal SAR interferometry reveals acceleration of bridge sinking before collapse. *Nat. Hazard. Earth Syst.* **2013**, *13*, 659–667. [[CrossRef](#)]
34. Gernhardt, S.; Auer, S.; Eder, K. Persistent scatterers at building facades evaluation of appearance and localization accuracy. *ISPRS J. Photogramm.* **2015**, *100*, 92–105. [[CrossRef](#)]
35. Hu, Q.W.; Wang, S.H.; Fu, C.W.; Ai, M.Y.; Yu, D.B.; Wang, W. Fine surveying and 3D modeling approach for wooden ancient architecture via multiple laser scanner integration. *Remote Sens.* **2016**, *8*, 270. [[CrossRef](#)]
36. Huang, H.; Li, Z.; Gong, P.; Cheng, X.; Clinton, N.; Cao, C.; Wang, L. Automated methods for measuring DBH and tree heights with a commercial scanning lidar. *Photogramm. Eng. Remote Sci.* **2011**, *77*, 219–227. [[CrossRef](#)]
37. Noferini, L.; Pieraccini, M.; Mecatti, D.; Luzi, G.; Atzeni, C.; Tamburini, A.; Broccolato, M. Permanent scatterers analysis for atmospheric correction in ground-based SAR interferometry. *IEEE Trans. Geosci. Remote Sens.* **2005**, *43*, 1459–1471. [[CrossRef](#)]
38. Negulescu, C.; Luzi, G.; Crosetto, M.; Raucoules, D.; Roullé, A.; Monfort, D.; Pujades, L.; Colas, B.; Dewez, T. Comparison of seismometer and radar measurements for the modal identification of civil engineering structures. *Eng. Struct.* **2013**, *51*, 10–22. [[CrossRef](#)]
39. Montuori, A.; Luzi, G.; Bignami, C.; Gaudiosi, I.; Stramondo, S.; Crosetto, M.; Buongiorno, M.F. The Interferometric Use of Radar Sensors for the Urban Monitoring of Structural Vibrations and Surface Displacements. *IEEE J. Sel. Top. Appl. Earth Observ. Remote Sens.* **2016**, *9*, 3761–3776. [[CrossRef](#)]
40. Beben, D. Application of the interferometric radar for dynamic tests of corrugated steel plate (CSP) culvert. *NDT E Int.* **2011**, *44*, 405–412. [[CrossRef](#)]
41. Salawu, O.S. Detection of structural damage through changes in frequency: A review. *Eng. Struct.* **1997**, *19*, 718–723. [[CrossRef](#)]
42. Crosetto, M.; Monserrat, O.; Luzi, G.; Cuevas-Gonzalez, M.; Devanthery, N. A noninterferometric procedure for deformation measurement using GB-SAR imagery. *IEEE Geosci. Remote Sens. Lett.* **2013**, *11*, 34–38. [[CrossRef](#)]
43. Wang, J.L.; Li, Z.J. Extreme-Point Symmetric Mode Decomposition Method for Data Analysis. *Adv. Adapt. Data Anal.* **2013**, *5*, 1137. [[CrossRef](#)]
44. Liu, X.; Tang, Y.; Lu, Z.; Huang, H.; Tong, X.; Ma, J. ESMD-based stability analysis in the progressive collapse of a building model: A case study of a reinforced concrete frame-shear wall model. *Measurement* **2018**, *120*, 34–42. [[CrossRef](#)]
45. Liu, X.; Lu, Z.; Yang, W.; Huang, M.; Tong, X. Dynamic Monitoring and Vibration Analysis of Ancient Bridges by Ground-Based Microwave Interferometry and the ESMD Method. *Remote Sens.* **2018**, *10*, 770. [[CrossRef](#)]
46. Chen, H.G.; Yan, Y.J.; Jiang, J.S. Vibration-based damage detection in composite wingbox structures by HHT. *Mech. Syst. Signal Process.* **2007**, *21*, 307–321. [[CrossRef](#)]
47. Wang, T.; Liao, M.; Perissin, D. InSAR coherence-decomposition analysis. *IEEE Geosci. Remote Sens. Lett.* **2010**, *7*, 156–160. [[CrossRef](#)]

